

## RESEARCH ARTICLE

10.1002/2014JC009816

## Physical and biological controls on oxygen saturation variability in the upper Arctic Ocean

Rachel Eveleth<sup>1</sup>, Mary-Louise Timmermans<sup>2</sup>, and Nicolas Cassar<sup>1</sup><sup>1</sup>Division of Earth and Ocean Sciences, Nicholas School of the Environment, Duke University, Durham, North Carolina, USA, <sup>2</sup>Department of Geology and Geophysics, Yale University, New Haven, Connecticut, USA

## Key Points:

- Biological and physical oxygen have interbasin variability in the Arctic
- Ar undersaturation in the Nansen Basin likely due to melt
- O<sub>2</sub>/Ar supersaturation indicates biological activity beneath ice cover

## Supporting Information:

- Readme
- Figure S1
- Figure S2

## Correspondence to:

R. Eveleth,  
rachel.eveleth@duke.edu

## Citation:

Eveleth, R., M.-L. Timmermans, and N. Cassar (2014), Physical and biological controls on oxygen saturation variability in the upper Arctic Ocean, *J. Geophys. Res. Oceans*, 119, 7420–7432, doi:10.1002/2014JC009816.

Received 14 JAN 2014

Accepted 2 OCT 2014

Accepted article online 6 OCT 2014

Published online 3 NOV 2014

**Abstract** Employing continuous in situ measurements of dissolved O<sub>2</sub>/Ar and O<sub>2</sub> in the Arctic Ocean, we investigate the mechanisms controlling the physical (abiotic) and biological oxygen saturation state variability in the surface ocean beneath sea ice. O<sub>2</sub>/Ar measurements were made underway using Equilibrator Inlet Mass Spectrometry (EIMS) during an icebreaker survey transiting the upper Arctic Ocean across the North Pole in late summer 2011. Using concurrently collected measurements of total oxygen, we devolve biological oxygen saturation and physical oxygen (Ar) saturation signals at unprecedented horizontal resolution in the surface ocean. In the Nansen Basin, Ar is undersaturated up to −7% while biological oxygen supersaturation peaks at 18.4%. We attribute this to ice melt, Atlantic Water influence and/or cooling. In the Canadian Basin, Ar is supersaturated up to 3%, likely because of Ar injection from freezing processes and long residence times of gas under ice cover. The overall Canadian Basin to Eurasian Basin gradient of Ar supersaturation to undersaturation may reflect net freezing in the Canadian Basin and net melting in the Eurasian Basin over several seasons, either by Pacific to Atlantic sector ice transport or local changes over time. Ar saturation could thereby provide large-scale high-resolution estimates of current and future changes in these processes. O<sub>2</sub>/Ar supersaturation averages 4.9% with peaks up to 9.8% where first year ice and abundant melt ponds likely allow sufficient light for blooms in ice-covered regions.

## 1. Introduction

Sea ice extent in the Arctic has rapidly declined in recent decades, while ocean temperatures have warmed, and many have speculated on how an evolving physical landscape may impact productivity [Arrigo *et al.*, 2008; Carmack *et al.*, 2006; Popova *et al.*, 2012; Tremblay *et al.*, 2011]. Critical to our prediction of future change in carbon cycling is a thorough understanding of biological-physical couplings today.

The biological oxygen (O<sub>2</sub>) saturation in the surface ocean records the relative contribution of photosynthesis and respiration and the exchange of biologically derived O<sub>2</sub> with the atmosphere (Figure 1). While it was once thought that only seasonally ice-free regions in the Arctic were productive, we now know phytoplankton blooms in surface waters under ice could provide a substantial contribution to total Arctic productivity [Arrigo *et al.*, 2012; Mundy *et al.*, 2009] and subsequently biological O<sub>2</sub> supersaturation. Additionally, sea ice harbors a large biological community, and the melting of sea ice seeds the water column with ice algae [Boetius *et al.*, 2013] and releases O<sub>2</sub> reflecting this sympagic biological activity.

Gas saturation state variability is driven by water property changes that affect solubility on shorter timescales than atmosphere-ocean equilibration. In the open ocean, equilibration timescales of O<sub>2</sub> are typically on the order of 10–14 days, depending on mixed-layer depths and piston velocity. Gas flux across the air-sea boundary is a function of diffusive mechanisms and bubble processes. In steady state, diffusion from the ocean to the atmosphere is balanced by a flux of gas into the ocean by diffusion and bubble processes [Emerson and Hedges, 2008].

Changes in atmospheric pressure, water temperature, and to a lesser extent salinity all affect gas solubility and drive saturation state deviations if they occur on shorter timescales than equilibration (Figure 1) [Hamme and Emerson, 2004; Spitzer and Jenkins, 1989]. Although it is not currently well constrained, sea ice growth, and decay also influence mixed-layer O<sub>2</sub> saturation through several processes [Hood *et al.*, 1998; Loose *et al.*, 2009]. O<sub>2</sub> is expelled from ice during freezing [Top *et al.*, 1985]. Further, sea ice cover limits gas exchange with the atmosphere [Loose *et al.*, 2014], likely increasing the residence time of O<sub>2</sub> in the mixed layer relative to open ocean conditions. There is little consensus at this time as to the scale of the effect,

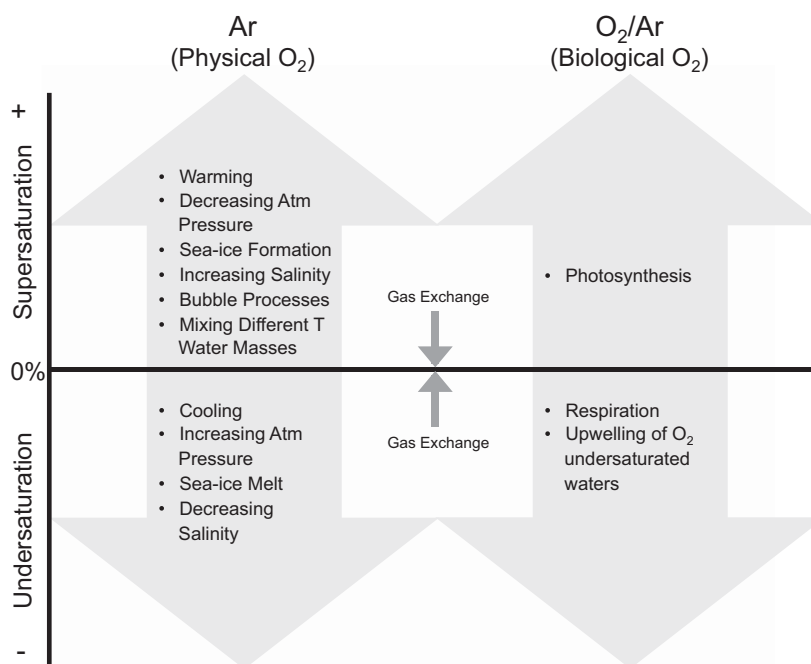


**Figure 1.** Processes driving Ar and O<sub>2</sub>/Ar saturation state toward supersaturation or undersaturation when occurring on shorter timescales than equilibration. Ocean-atmosphere gas exchange works toward equilibrium.

with estimates ranging from total [Poisson and Chen, 1987] to slight reduction in gas exchange [Fanning and Torres, 1991]; of course, the presence of cracks or openings (leads) in the sea ice pack is likely to have a significant local influence on surface-ocean O<sub>2</sub> concentrations. Estimates of gas exchange based on <sup>222</sup>Rn/<sup>226</sup>Ra ratio measurements taken during the same 2011 icebreaker survey as the measurements analyzed in this paper indicate that the presence of even 56% sea ice cover substantially reduces gas exchange by an order of magnitude or more [Rutgers van der Loeff et al., 2014]. This would have the effect of increasing the residence time of O<sub>2</sub> in the surface ocean to weeks to months under the ice and in parts of the marginal ice zone (MIZ).

The physical processes described above presumably affect O<sub>2</sub> and Ar in roughly the same way because the two gases have very similar solubility properties [Craig and Hayward, 1987]. In this analysis, we exploit the similar physical properties of O<sub>2</sub> and Ar to separate biological and physical oxygen saturation state changes. Because Ar is inert we are able to use the ratio of O<sub>2</sub> to Ar (i.e., O<sub>2</sub>/Ar) to infer biological oxygen supersaturation and Ar to infer physical oxygen supersaturation, where the latter represents abiotic supersaturation as would be observed in a sterile ocean. We use continuous records of both total oxygen concentration and O<sub>2</sub>/Ar across the Arctic Ocean during the late summer of 2011 to extract these biological and physical signals.

While there have been many studies of total oxygen saturation in the Arctic, attempts to separate biological and physical impacts on this total signal have been largely speculative [Codispoti and Richards, 1971; Falkner et al., 2005; Timmermans et al., 2010]. Our extensive data (measurements are made at an unprecedented O(1 km) horizontal resolution for thousands of kilometers across the Arctic Ocean) are analyzed here to assess the magnitude, variability, and coupling of biological O<sub>2</sub> and physical O<sub>2</sub> saturation states across the Arctic, and to show that the controlling mechanisms of saturation vary regionally, with potential implications for future conditions.

## 2. Methods

Biological O<sub>2</sub> supersaturation was quantified by measuring O<sub>2</sub>/Ar in the mixed layer using in situ continuous Equilibrator Inlet Mass Spectrometry (EIMS) [Cassar et al., 2009]. Briefly, water from the ship's underway flow through system, at ~8 m depth, entered the EIMS system and was pumped through silver tygon tubing, a series of filters to remove particulates and to a gas-permeable membrane contactor cartridge

(MicroModule<sup>®</sup> 0.75 × 1) where the air in the headspace equilibrated with the dissolved gases in the water of the cartridge. That air was sent via a fused silica capillary to a quadrupole mass spectrometer (Pfeiffer Prisma model QMG 220 M1) for measurement of dissolved gases. Measurements were recorded every 8 s and later averaged into 2 min intervals. The system calibrates by switching to sample the atmosphere via an open silica capillary for 20 min every 4 h. We did not observe significant depletion of O<sub>2</sub> in the lines of the ship as confirmed by bottle samples (data not shown). The instrument precision is ±0.3% or better [Cassar *et al.*, 2009]. The e-folding response time is 7.75 ± 0.25 min [Cassar *et al.*, 2009]. We do not use O<sub>2</sub>/Ar to calculate net community production (NCP) in this study; however, Ulfsbo *et al.* [2014] found in an NCP comparison study good agreement between O<sub>2</sub>/Ar-NCP estimates and nutrient-based NCP estimates during this same cruise in the upper Arctic Ocean.

Total O<sub>2</sub> concentration was measured continuously using an Aanderaa Optode Model 4835 (sensor response time <25 s) every 30 s. Optode measurements were calibrated against discrete Winkler titrations according to the method of Uchida *et al.* [2008] (supporting information Figure S1). Optode oxygen measurements are representative of total oxygen in the mixed layer. Additional optode measurements taken at the ship's seawater intake were consistent with these values and give the same Ar saturation trends and magnitude.

It is commonly accepted that the ratio of physical O<sub>2</sub> concentration to O<sub>2</sub> concentration at saturation is equal to the ratio of Ar concentration to Ar concentration at saturation [Cassar *et al.*, 2011; Craig and Hayward, 1987]. We assume that the solubility properties of O<sub>2</sub> and Ar derived under standard conditions hold under the conditions encountered during our cruise, but future studies should verify the applicability in brine and freezing temperatures of the surface ocean sampled here.

Total O<sub>2</sub> concentration ([O<sub>2</sub>]<sub>total</sub>) is the sum of the oxygen concentration at equilibrium saturation ([O<sub>2</sub>]<sub>sat</sub>), biological O<sub>2</sub> concentration ([O<sub>2</sub>]<sub>bio</sub>), and physical O<sub>2</sub> concentration in excess of saturation ([O<sub>2</sub>]<sub>phys</sub>). Ar supersaturation (ΔAr) is given as

$$\Delta Ar = \frac{[Ar]}{[Ar]_{sat}} - 1 \tag{1}$$

and we can thus define

$$[O_2]_{phys} = \Delta Ar [O_2]_{sat} \tag{2}$$

These give

$$[O_2]_{bio} = \frac{[Ar]}{[Ar]_{sat}} [O_2]_{sat} \Delta(O_2/Ar) \tag{3}$$

where we have introduced

$$\Delta(O_2/Ar) = \left[ \frac{([O_2]_{total}/[Ar])}{([O_2]/[Ar])_{sat}} - 1 \right] \tag{4}$$

This is typically considered to be the biological oxygen supersaturation under the assumption [Ar]/[Ar]<sub>sat</sub> = 1 [Cassar *et al.*, 2011]. Alternatively, ΔAr can then be estimated as follows:

$$\Delta Ar = \Delta(O_2)_{total} - \frac{[Ar]}{[Ar]_{sat}} \Delta(O_2/Ar) \tag{5}$$

ΔAr is equal to the physical oxygen supersaturation, under the observed temperature, salinity, and mixing conditions and the terms are used interchangeably hereafter. All supersaturations were multiplied by 100 and are reported here in percent. We backed out [Ar] from EIMS measurements of Δ(O<sub>2</sub>/Ar) using [O<sub>2</sub>]<sub>total</sub> from optode measurements and the equilibrium saturation concentrations of O<sub>2</sub> ([O<sub>2</sub>]<sub>sat</sub>) and Ar ([Ar]<sub>sat</sub>). [O<sub>2</sub>]<sub>sat</sub> and [Ar]<sub>sat</sub> were calculated using the equations of Garcia and Gordon [1992] and Hamme and Emerson [2004], respectively, and were corrected for atmospheric pressure by multiplying the ratio of observed sea-level pressure as measured by shipboard sensors underway to standard pressure. In calling Δ(O<sub>2</sub>/Ar) biological oxygen supersaturation, we assume Ar is at equilibrium saturation. By making this assumption, we are introducing an error in Δ(O<sub>2</sub>)<sub>bio</sub> that is equal to the observed Ar supersaturation. This does not alter the more qualitative discussion of Δ(O<sub>2</sub>)<sub>bio</sub> presented here, but is an important note for calculations of NCP

when Ar saturation deviates substantially from saturation (e.g., brine where Ar undersaturation may be as low as 45%) [Top *et al.*, 1988]. In a recent study by Shadwick *et al.* [2014], physical oxygen supersaturation was calculated by the difference between  $\Delta(\text{O}_2)_{\text{total}}$  and  $\Delta(\text{O}_2/\text{Ar})$  assuming the latter represents  $\Delta(\text{O}_2)_{\text{bio}}$ . While this is reasonable in open water where Ar is typically within 1% of saturation, this approach propagates the error in  $\Delta(\text{O}_2)_{\text{bio}}$  into the  $\Delta\text{Ar}$  calculations, which can be significant in regions with strong argon super(under)saturation.

Temperature and salinity were measured underway at the ship's keel (11 m depth) where there is relatively little impact of ship-induced mixing or warming in the intake [Schauer *et al.*, 2012]. We removed all data from the record during times when the ship was held at station (traveling slower than two knots) because active thruster and propeller mixing may disturb the upper layer at these times. It is also possible that as the ship broke ice it released the by-products of the ice rubble field into the surface water, altering gas, and T-S properties, but this likely had a small influence and we do not account for this here. Cumulative distance traveled was calculated from the distance between each 2 min averaged data point and all data were interpolated to a 1.2 km grid to account for varying response times of the measurements and an average ship speed of approximately five knots (0.15 km/min). Full water column CTD measurements were taken at 136 hydrographic stations using a SBE911 mounted on the Polarstern's CTD-rosette system [Schauer *et al.*, 2012], and nutrients were analyzed from rosette bottle samples (G. Kattner, personal communication, 2013, see Ulfso *et al.* [2014] for nutrient sampling and analysis details).

An assessment of meltwater concentration is important for understanding gas saturation state drivers; gas expulsion during freezing leads to meltwater that is undersaturated. Meltwater content was estimated by two independent methods. The first is given by Korhonen *et al.* [2013] who used ocean temperature and salinity profiles to infer melt. These authors approximated summer melt input as the difference between the salinity at the depth of the submixed-layer temperature minimum (that traces the remnant winter mixed layer) and the mixed-layer salinity. The hydrographic meltwater estimates from Korhonen *et al.* [2013] are in linear agreement ( $r^2 = 0.81$ , supporting information Figure S2) with an independent mass balance based meltwater estimate completed in this study. We employed the fraction of Pacific water from Rutgers van der Loeff *et al.* [2014] and Atlantic and Pacific source water characteristics from Ekwurzel *et al.* [2001] to estimate an upper bound on accumulated meltwater using a simple mass balance. Both methods are limited in their ability to discriminate between meltwater and other sources of freshwater change (e.g., river input and dynamical ocean variability). In the Canadian Basin, much of the freshwater content variability is a result of wind driven surface flow of the Beaufort Gyre accumulating melt and riverine input [Proshutinsky *et al.*, 2009]. These accumulated freshwaters could appear as meltwater in calculations but may be less Ar undersaturated than if they were completely sourced from melting ice. Thus, in this region, any expected relationship between  $\Delta\text{Ar}$  and meltwater is likely to be obscured. Meltwater estimates using the hydrographic temperature minimum method of Korhonen *et al.* [2013] are presented throughout the remainder of the text because they have the best spatial coverage.

### 3. Study Area

Dissolved  $\text{O}_2$ , temperature, and salinity measurements were taken via the underway system of the R/V Polarstern from August to September 2011 as part of the TransArc cruise (ARK-XXVI/3). Our measurements began on August 10 just north of Franz Josef Land in the Nansen Basin (NB), followed the 60°E line across the Amundsen Basin (AB) to the North Pole into the Makarov Basin (MB), then the northern Canada Basin (NCB) and returned to the NB before entering the ice-free Laptev Sea on 17 September (Figure 2). Here we focus on this 4200 km, 38 day record that spans the 2011 annual sea ice minimum extent on 9 September (Figure 3). We mostly discuss our observations in the context of regional variations. However, we note that seasonal processes may affect the observed patterns, albeit to a lesser extent than in the open ocean because of the longer residence time of gases under sea ice. The uncertainty in under ice residence time provides additional challenges when we interpret our signals because we are seeing the cumulative effects of processes over longer periods of time. For example, barometric pressure history could have a significant impact on the physical supersaturation. One could correct for atmospheric pressure history [Shadwick *et al.*, 2014] but such a correction is only possible with knowledge of the residence time of  $\text{O}_2$  in the surface ocean in sea ice-covered regions.

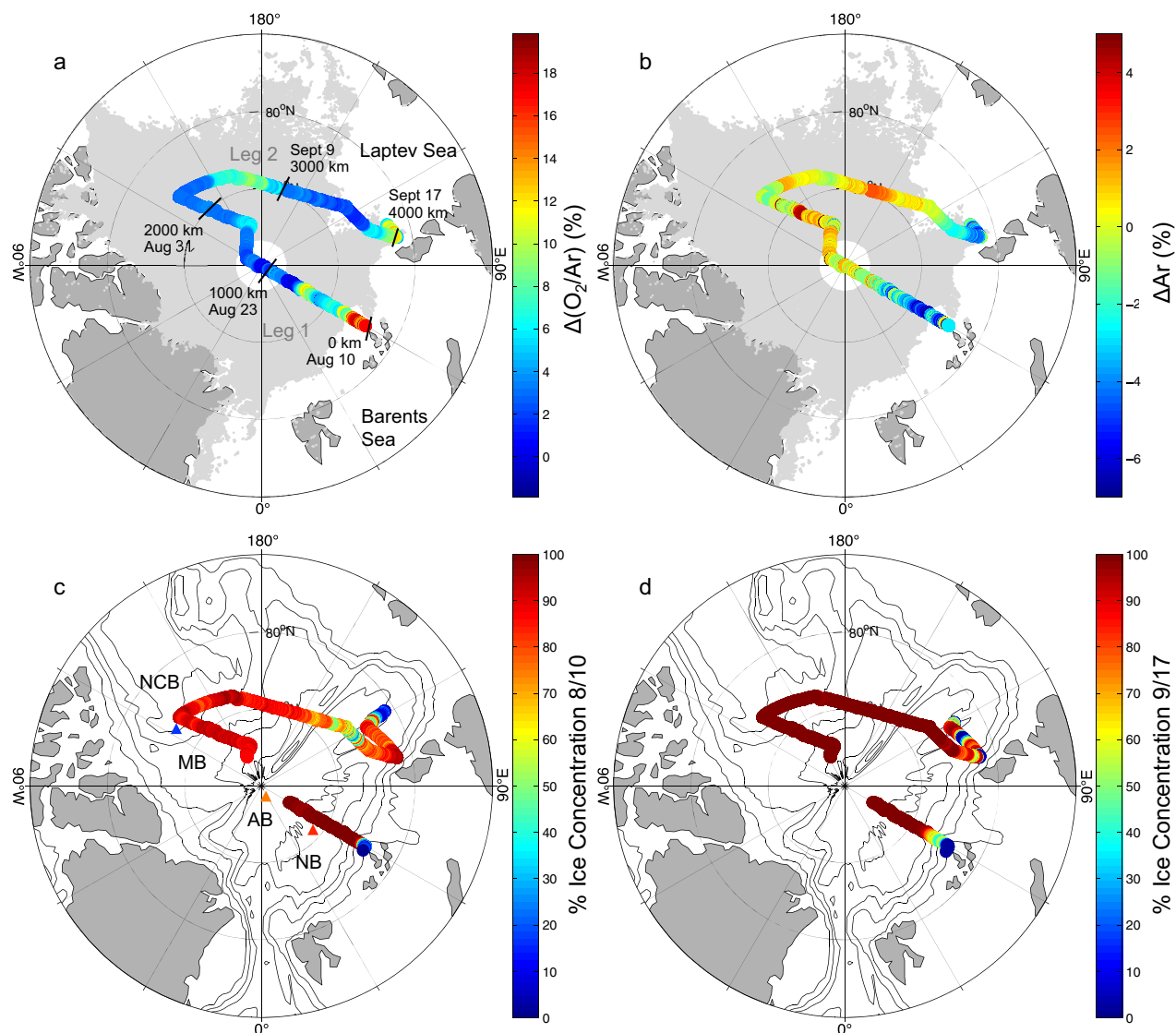


**Figure 2.** (a) Biological oxygen supersaturation % ( $\Delta(O_2/Ar)$ ) and (b) Ar supersaturation ( $\Delta Ar$ ), a proxy for physical oxygen supersaturation %, for the full cruise track. Light gray-shaded region is the 2011 minimum sea ice extent defined by greater than 70% ice cover reached on September 9 from AMSR-E-derived sea ice. Distances correspond to cumulative distance in Figure 3. Percent ice cover along the cruise track from AMSR-E satellite measurements on (c) 10 August (when ship entered the ice) and (d) 17 September (when ship exited the ice). Basins indicated left: Nansen Basin (NB), Amundsen Basin (AB), Makarov Basin (MB), and Northern Canada Basin (NCB). Red, orange, and blue triangles mark locations of nutrient profiles in Figure 4b.

During the survey, a transition from 0% to 80–100% ice concentration (i.e., the marginal ice zone (MIZ)) was observed in the NB in AMSR-E satellite ice measurements (Figures 2c and 2d) [Spreen *et al.*, 2008] and as estimated from R/V Polarstern bridge observations using Arctic adapted standardized protocol (ASPeCT) [Nicolaus *et al.*, 2012; Worby *et al.*, 2008]. Satellite and shipboard sea ice observations show good agreement. For both methods, sea ice concentrations in the AB and Canadian Basin (MB and NCB) were between 80% and 100% for the entire cruise duration. In mid-late September during the return AB transit, ice concentrations had a minimum of 40%, with a transition to ice free conditions for the final portion of the survey in the eastern NB.

In the Eurasian Basin (NB and AB), the ocean summer mixed layer extends from the surface to a strong seasonal halocline at  $\sim 20$  m created by summer ice melt. An underlying remnant winter mixed layer, remaining from the previous winter's mixed layer, is a characteristic of this time of year and is identified by a temperature minimum at  $\sim 50$ – $80$  m. A 75–100 m thick halocline underlies the remnant winter mixed layer separating surface waters from the Atlantic Water (AW) core at 150–200 m. The halocline waters in this region are believed to be formed by surface buoyancy fluxes (e.g., cold dense flows generated by ice growth and subsequent brine rejection), including modification of inflowing AW [Rudels *et al.*, 2004; Steele

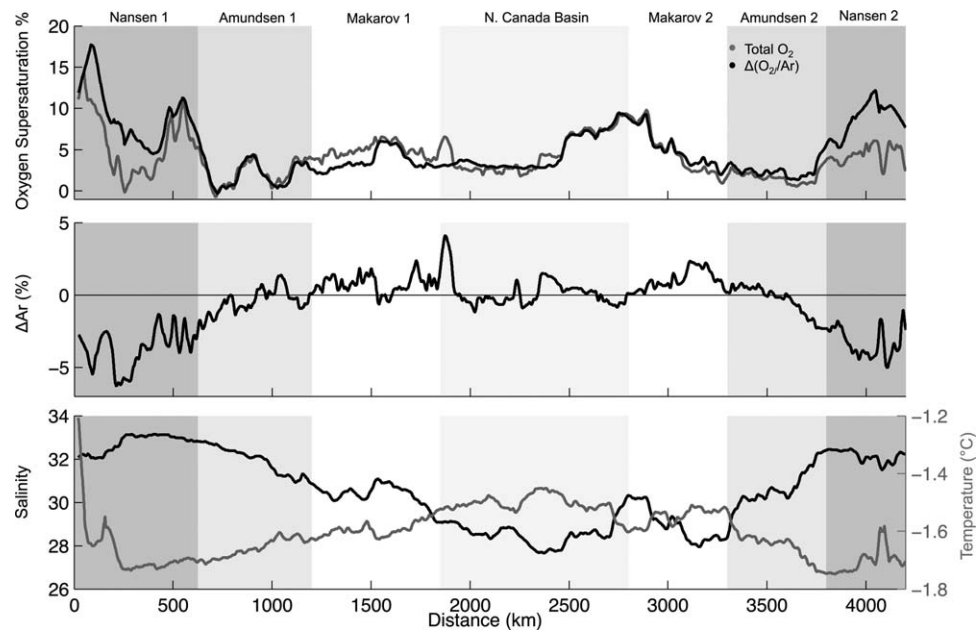


**Figure 3.** Distance series of optode-derived total O<sub>2</sub> supersaturation and EIMS-derived biological O<sub>2</sub> supersaturation, Ar supersaturation, salinity, and temperature interpolated on a 1.2 km grid then smoothed using the robust loess method [Cleveland, 1979].

and Boyd, 1998; Woodgate *et al.*, 2001]. Similar upper ocean structure is observed in the Makarov and Northern Canada Basins in summer, although with more influence from Pacific origin water. A ~20 m deep summer mixed layer and a remnant winter mixed layer ~50 m depth overlay water of Pacific origin. The lower halocline (~150 m depth) separates the fresher Pacific derived layer from the deep AW. Mixed-layer depths over the course of the survey were spatially and temporally variable with no clear differences between basins; nor were there any clear differences between the strength of the stratification at the base of the mixed layer. Defining the mixed-layer base by the depth of the maximum vertical density gradient in the upper 40 m, NB mixed layers were found to be  $22 \pm 6$  m, AB  $18 \pm 5$  m, MB,  $19 \pm 6$  m, and NCB  $20 \pm 5$  m. No apparent relationships between gas concentrations and mixed-layer depths were observed.

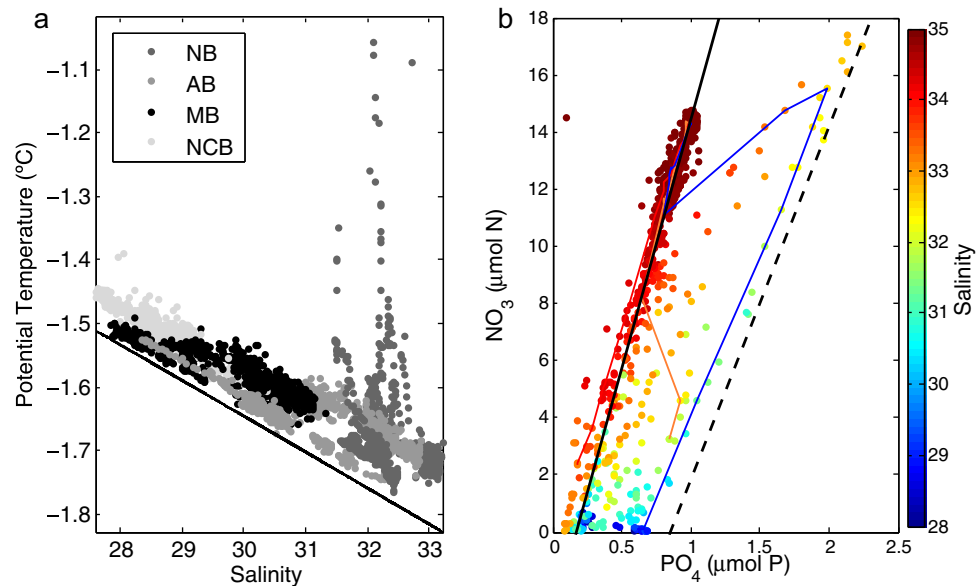


**Figure 4.** (a)  $\theta$ -S at 11 m colored by basin. Solid line is the freezing temperature. (b) Nitrate versus phosphate with salinity shown by the color scale for full depth profiles in all basins. Representative basin profiles at locations marked in Figure 2c: NB (red), AB (orange), and NCB (blue). Solid black line and dotted line in Figure 4b are the theoretical end member ratios for Atlantic and Pacific source waters, respectively, from Jones *et al.* [1998].

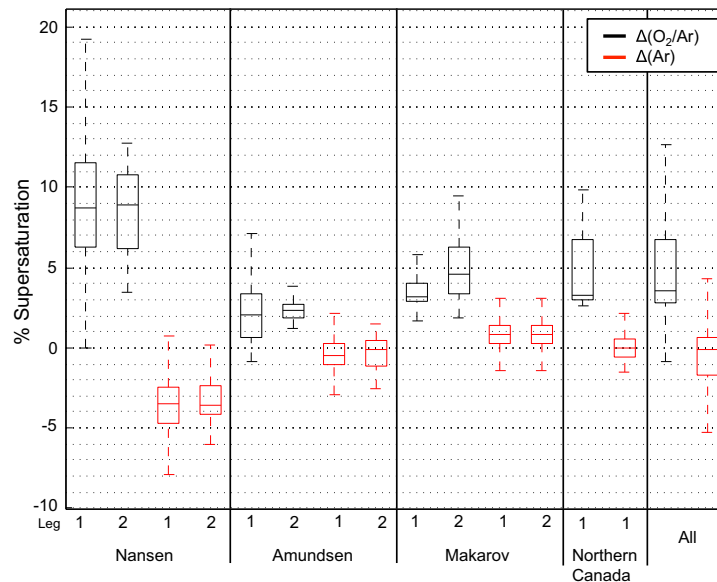


**Figure 5.**  $\Delta(\text{O}_2/\text{Ar})$  (black) and  $\Delta\text{Ar}$  (red) sectioned by basin and leg as denoted in Figure 3. Leg 1 was 10 August to 3 September, leg 2 4–17 September. Outliers, defined as values greater than  $\pm 2.7\sigma$ , are not shown.

Surface ocean temperatures are close to the freezing point under the ice in all basins (Figure 4a), with generally warmer temperatures in the Canadian Basin than in the Eurasian Basin because the Canadian Basin is fresher. The largest departure from freezing temperatures occurs in the NB MIZ where incoming solar radiation warms the surface ocean to above freezing. Eurasian Basin and Canadian Basin surface waters show characteristic variation in the nitrate:phosphate (N:P) relation owing to differing source waters, i.e., differing river inputs and influences from the Pacific and Atlantic oceans (Figure 4) [Jones *et al.*, 1998].

## 4. Results and Discussion

### 4.1. Overall Patterns

Averaged over the full record,  $\Delta\text{Ar}$  (i.e., physical oxygen supersaturation) is near equilibrium ( $-0.59 \pm 2.1\%$ ) and  $\Delta(\text{O}_2/\text{Ar})$  (i.e., biological oxygen supersaturation) is positive ( $4.98 \pm 3.4\%$ ). The mean of the ratio of  $\Delta(\text{O}_2/\text{Ar})$  to total  $\text{O}_2$  supersaturation is 1.09 while the mean of the ratio of  $\Delta\text{Ar}$  to total  $\text{O}_2$  supersaturation is  $-0.09$  (see also Figure 5). These observations suggest that, overall, the contribution of biological oxygen saturation dominates the mean total oxygen saturation ( $4.24 \pm 2.7\%$ ) over our measurement record. However, the magnitude of variability in  $\Delta\text{Ar}$  and  $\Delta(\text{O}_2/\text{Ar})$  is substantial (see discussion below).

$\Delta(\text{O}_2/\text{Ar})$  and  $\Delta\text{Ar}$  in the NB display no considerable difference between surveys during 10–15 August (NB leg 1) and during 14–17 September (NB leg 2) (Figure 5). On the other hand, large variations are observed between basins. The NB has large positive  $\Delta(\text{O}_2/\text{Ar})$  and negative  $\Delta\text{Ar}$ , while the Canadian Basin has relatively low  $\Delta(\text{O}_2/\text{Ar})$  and  $\Delta\text{Ar}$  that is near equilibrium or slightly positive (Figure 5). In some regions,  $\Delta(\text{O}_2/\text{Ar})$  and  $\Delta\text{Ar}$  are distinctly anticorrelated, while in other regions the two appear uncoupled. In the next section, we describe potential driving mechanisms of this basin-scale variability.

### 4.2. Basin-Scale Variability

#### 4.2.1. Eurasian Basin

The highest biological oxygen saturation (18.4%) and the lowest inferred physical oxygen undersaturation (i.e.,  $\Delta\text{Ar} = -7.1\%$ ) were measured in the NB (Figure 5). The two measurements display anticorrelated variability ( $r^2 = 0.52$ ), which is consistent with a common control mechanism. The NB is distinct from the other basins surveyed because it is influenced by (1) the summer MIZ, (2) the continental shelf break, and (3) the shallowest inflows of warm, salty Atlantic Waters [Lien *et al.*, 2013]. The AW influence is apparent in the high N:P ratio and high salinity (Figure 4b). Assuming physical oxygen initially near equilibrium saturation (i.e.,  $\Delta\text{Ar} \approx 0$ ), the observed  $\Delta\text{Ar}$  of  $-7.1\%$  could be achieved by any one of the following: 1.6 m of meltwater input in the upper 10 m, a 71 mbar increase in sea level pressure, 2.9°C surface-ocean cooling, or a 9.4 decrease in surface-ocean salinity. This is assuming no gas exchange with the atmosphere and that each

mechanism is acting in isolation; of course, a combination of these processes is a more likely scenario and some gas exchange is likely occurring in the marginal ice zone. It is conceivable that differences in local gas exchange due to variable ice cover could explain some of the kilometer-scale spatial variability in  $\Delta\text{Ar}$ ; however, in this survey, ship transit times across gas fronts and lateral gradients were much shorter than equilibration timescales. To set bounds on the maximum effect gas exchange could have on  $\Delta\text{Ar}$  in the NB we consider the first  $\sim 100$  km of the cruise track which became ice free fewer than 5 days prior to sampling and assume a piston velocity of  $0.5 \text{ m d}^{-1}$  (as given for analogous conditions in *Rutgers van der Loeff et al.* [2014]). Multiplying this coefficient by the Ar concentration gradient, starting with the observed concentration, and updating the concentration gradient at each daily time step for 5 days gives a decrease in the  $\Delta\text{Ar}$  undersaturation of 0.5%. In low sea ice concentrations gas exchange with the atmosphere will reduce the amplitude of the lateral variability; however, these effects are expected to be smaller than the observed spatial signal especially over most of the transect with close to 100% ice cover. Below, we discuss AW influence and sea ice melt as the most likely drivers of the observed high  $\Delta(\text{O}_2/\text{Ar})$  and negative  $\Delta\text{Ar}$  in the NB.

#### 4.2.1.1. AW Influence

Upon entering the Arctic Ocean, the AW encounters the sea ice edge and induces melting; subsequent cooling, freezing, and mixing (convective and shear-driven) modify the AW and maintain the cold halocline [*Rudels et al.*, 1996]. Therefore, the upper waters in this region have a significant fraction of transformed AW. Further, AW that resides below the surface layers is known to penetrate the surface of the NB directly (with subsequent heat losses) when forced by upwelling favorable winds [*Lind and Ingvaldsen*, 2012; *Rudels et al.*, 1994; *Schauer and Beszczynska-Möller*, 2009]. Although no direct evidence for upwelling was observed here, NCEP reanalysis fields show upwelling favorable easterly winds were present along the shelf break from August to September 2011 consistent with typical patterns [*Overland et al.*, 2011] although meridional winds were quite variable over this time. It is of importance that AW is a source of nutrients to the Arctic [*Garcia et al.*, 2010] and AW influence at the surface could explain the observed biological oxygen supersaturation and physical oxygen undersaturation by (1) promoting primary productivity and (2) AW cooling at the surface. *Moore and Spitzer* [1990] previously analyzed Ar concentrations at depth in the region to infer AW cooling in the Arctic Ocean due to communication with sea ice at the surface. Here we examine the Ar signal in the surface ocean of the NB to infer its origins. In the extreme scenario that the surface ocean layer derived entirely from upwelled AW, we would expect an Ar undersaturation of  $-11.6\%$ , almost double the largest undersaturations measured here. This is based on the assumption that AW was initially at saturation and subsequently cools and freshens to the observed summer mixed layer values (based on the upper ocean temperature and salinity measurements in the NB); this further assumes no gas exchange with the atmosphere nor any meltwater input. In the absence of sea ice, undersaturation would be reduced by gas exchange and equilibration with the atmosphere, which could occur on timescales of  $\sim 10$ – $14$  days. In the ice-covered NB, equilibration timescales are  $\sim 160$ – $280$  days (based on a  $22 \pm 6$  m MLD and  $0.1 \text{ m d}^{-1}$  piston velocity) [*Rutgers van der Loeff et al.*, 2014], so the observed spatial variability can primarily be attributed to biological and physical processes that are acting faster than gas exchange is able to erase the signal. Larger undersaturations would result for AW that was initially Ar undersaturated, which could be the case if there was low atmospheric pressure at the time AW was isolated from the surface [*Moore and Spitzer*, 1990]. Of course, we cannot rule out the possibility of Ar supersaturated source waters such as if wave breaking and bubble injection were strong prior to isolation from the surface.

Over the Gakkel Ridge, there are elevated nutrient concentrations in the remnant winter water just below the mixed layer and it is possible that these nutrients are being mined to create the elevated  $\Delta(\text{O}_2/\text{Ar})$  above the ridge.

#### 4.2.1.2. Meltwater

Given the low likelihood of all other undersaturating mechanisms, we conclude that ice melt is the most plausible explanation for the low  $\Delta\text{Ar}$  in the NB. Meltwater is  $\sim 45\%$  Ar undersaturated as a result of exclusion of Ar from the ice lattice during freezing [*Top et al.*, 1988]. This approximation does not account for Ar flux to the atmosphere [*Moreau et al.*, 2014] and is likely quite variable, although the trend of the impact remains the same in the estimates that follow. Additionally, although it is a smaller effect, melting causes freshening which, without gas exchange, leads to Ar undersaturation. The expected inverse relationship between meltwater and  $\Delta\text{Ar}$  is consistent with our observations in the NB during occupations in both August and September (Figure 6). Given a maximum meltwater input of 0.65 m in the upper 10 m as

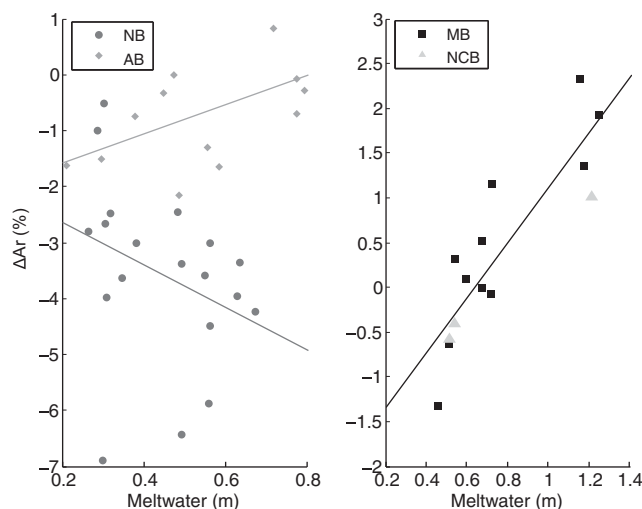


**Figure 6.** Ar supersaturation versus meltwater in the upper 10 m [Korhonen *et al.*, 2013] in (left) the Eurasian Basin and (right) the Canadian Basin. Linear regression shows negative relationship in the NB ( $r^2 = 0.11$ , circles left) and positive in the AB ( $r^2 = 0.27$ , diamonds left) and Canadian Basins ( $r^2 = 0.76$ , right).

observed in the NB (Figure 6), and assuming (for lack of measurement) initial  $\Delta\text{Ar}$  at equilibrium, the largest negative  $\Delta\text{Ar}$  that could occur from meltwater input alone is  $\sim -3\%$ . The associated freshening would further reduce the saturation by an additional  $\sim -1\%$ . These values are comparable in general to the observed Ar-meltwater relation in the Nansen Basin but cannot explain the strong undersaturation ( $< -5\%$ ) in the first 300 km of the cruise (Figure 6). Underestimation of the  $\Delta\text{Ar}$  undersaturation or meltwater volume and/or AW influences may also play a role. Meltwater estimates using the simple mass balance

method are unavailable for the Nansen Basin due to a lack of nutrient data, but assuming the linear relationship with the hydrographic estimates of Korhonen *et al.* [2013] hold, meltwater content could be up to 1.3 m. If meltwater input is closer to 1.3 m in the upper 10 m then the flux of this Ar undersaturated and relatively fresh water could produce  $\Delta\text{Ar} \sim -8.6\%$  ( $-6\%$  from undersaturated input and  $-2.6\%$  from freshening) exceeding the value observed. Additionally,  $\Delta\text{Ar}$  could be reflecting net melting in the Nansen Basin over several seasons [Ekwrzel *et al.*, 2001; Newton *et al.*, 2013].

Melting could also explain the peaks in  $\Delta(\text{O}_2/\text{Ar})$  that we observe in the Nansen Basin. Ice-edge phytoplankton blooms are well documented in the Arctic [Mundy *et al.*, 2009; Perrette *et al.*, 2011]. As ice retreats, strong stratification and increased light levels favor bloom conditions. These blooms may be preconditioned by low-level under ice production and underutilized nutrients [Vancoppenolle *et al.*, 2013]. We must also consider the sympagic biological community [Boetius *et al.*, 2013; Horner *et al.*, 1992] which could lead to biological oxygen supersaturation in the ice that is then released into the mixed layer during melting. Discrete measurements of brine water extracted from sea ice at eight stations during the transect were performed in Rachel Stanley's lab (WHOI) and yielded an average  $\Delta(\text{O}_2/\text{Ar})$  of  $9.1 \pm 6.8\%$  in the ice. To obtain an upper bound on the resulting surface ocean  $\Delta(\text{O}_2/\text{Ar})$ , we assume that 100% of meltwater derived from 9.1% supersaturated brine. This yields a maximum  $\Delta(\text{O}_2/\text{Ar})$  of 3.2% in the mixed layer given 0.65 m of meltwater in the upper 10 m. Brine  $\Delta(\text{O}_2/\text{Ar})$  would need to be at least 150% supersaturated to explain the 19% mixed layer supersaturation we observe. Perhaps surprisingly, this is within the range of recently documented high in-ice biological  $\text{O}_2$  in a highly productive Arctic sector near Barrow Alaska [Zhou *et al.*, 2014] although these high saturations were not observed on our transect. While 3.2% is a small contribution to the 19%  $\Delta(\text{O}_2/\text{Ar})$  we measured, premelt sympagic algae could be seeding the phytoplankton activity that is likely driving the high  $\Delta(\text{O}_2/\text{Ar})$  in the MIZ [Michel *et al.*, 1993; Tedesco *et al.*, 2012]. The high remaining biological oxygen contribution suggests sufficient nutrients for in situ production. Under ice cover, where gas exchange is slow, a small excess of photosynthesis over respiration could lead to the observed  $\Delta(\text{O}_2/\text{Ar})$  signal when integrated over the long residence times of  $\text{O}_2$ . If melt is the main driver of the negative  $\Delta\text{Ar}$  and high positive  $\Delta(\text{O}_2/\text{Ar})$ , we might expect similar signals in the MIZs of the other basins.

Finally, it is instructive to point out here that we see variability on smaller scales that is consistent with upper ocean processes. For example, during leg 1, the ice edge was located at  $\sim 84.1^\circ\text{N}$  and  $59.9^\circ\text{E}$  (at  $\sim 200$  km) coincident with a surface ocean front between relatively warm fresh surface waters to the south, and cooler, saltier surface waters to the north (Figure 7). South of the front the upper 10 m contains a relatively high meltwater component; reduced ice cover here means greater ocean-atmosphere gas exchange than on the north side of the front, presumably driving undersaturation in the surface waters toward

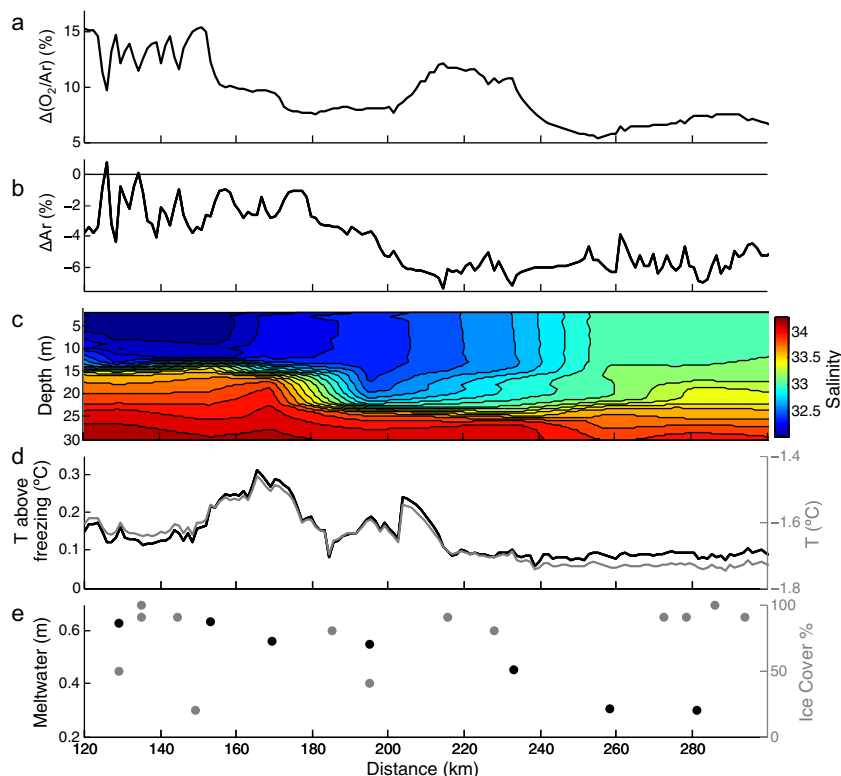


**Figure 7.** (a)  $\Delta(O_2/Ar)$ , (b)  $\Delta Ar$ , (c) salinity with depth interpolated from CTD measurements, (d) underway 11 m temperature above freezing and underway 11 m temperature, and (e) meltwater in the upper 10 m and % ice cover estimated from bridge observations all in the vicinity of a surface front in the Nansen Basin.

equilibrium. In the vicinity of the front,  $\Delta Ar$  is the lowest measured anywhere in the survey and this minima is coincident with a local maxima in  $\Delta(O_2/Ar)$ . This enhanced biological activity may be related to complex 3-D circulation dynamics in the frontal region [D'Asaro *et al.*, 2011] that supply a fresh source of nutrients from deeper waters.

#### 4.2.1.3. Amundsen Basin

The Amundsen Basin shows  $\Delta Ar$  near equilibrium or slightly negative ( $-0.35 \pm 1.2\%$ ), and appears to be a transitional zone between the Canadian Basin and the NB. The peak  $\Delta Ar$  (2.5%) in this basin occurs near the North Pole, where a low N:P ratio at the surface resembles that characterizing Pacific water (Figure 4b). The Pacific Water influence in this region is consistent with surface circulation [Falkner *et al.*, 2005; Jones *et al.*, 1998, 2008]. It is possible that surface circulation is transporting Ar supersaturated Canadian Basin waters into the Amundsen Basin.

#### 4.2.2. Canadian Basin

In the Canadian Basin,  $\Delta Ar$  is near equilibrium or positive (up to 3%).  $\Delta Ar$  variability is not well correlated ( $r^2 = 0.06$ ) with variability in biological oxygen supersaturation ( $\Delta(O_2/Ar)$  with values up to 9.8%). Following our previous reasoning, assuming no gas exchange with the atmosphere, to obtain 3% Ar supersaturation (from an initial equilibrium) any one of the following mechanisms could be invoked: a sea level pressure decrease of 30 mb,  $1.1^\circ$  warming or a 3.8 salinity increase. Bubble processes are assumed to be negligible under the extensive sea ice cover in the Canadian Basin when the measurements were taken. Assuming negligible gas exchange is likely valid here as Rutgers van der Loeff *et al.* [2014] found that gas exchange velocity in these ice-covered regions was  $< 0.1 \text{ m d}^{-1}$ , giving a residence time of at least 200 days. It is possible that bubble processes could create source water supersaturation at a disparate location or time. Additionally, mixing of two different temperature water masses is not dynamically likely here and would require an unreasonably high temperature difference. None of these processes seem to be likely drivers of the small Ar supersaturation based on observed conditions.

It is most likely that sea ice conditions (i.e., freezing and exclusion of Ar from ice) are a primary control of  $\Delta Ar$  in this basin. As the R/V Polarstern transited the Canada, Makarov, and Eastern Amundsen Basins along

the ship track sea ice concentrations ranged from 70–90% to 100%. Bridge observations document freezing conditions beginning on 22 August, when melt ponds were beginning to freeze over. Note, however, that AMSR-E satellite measurements suggest the Arctic wide sea ice minimum extent for 2011 was reached on 9 September (nsidc.org). Satellite ice measurements additionally cannot sense grease ice and frazil ice, which were observed from the bridge to cover up to 10% [Nicolaus *et al.*, 2012] and would also influence the gas saturation. Based on a freezing degree days model [Anderson, 1961], ~10 cm of ice grew between 31 August and 13 September (M. Rutgers van der Loeff, personal communication, 2013). If this estimate is correct, then freezing would have a negligible effect on Ar supersaturation in the mixed layer. However, it is conceivable that the observed Ar supersaturation could be a product of net freezing during the previous winter and subsequent gas trapping by extensive multiyear sea ice cover [Timmermans *et al.*, 2010] as shipboard observations suggest throughout much of the Canadian Basin [Nicolaus *et al.*, 2012]. Finally, we point out here that  $\Delta Ar$  in the surface Canadian Basin is strongly positively correlated with meltwater estimates (Figure 6b), opposite to the expected relationship given that meltwater is undersaturated. The same meltwater estimates are weakly anticorrelated with surface ocean salinity, which is consistent with the general trend of increasing Ar concentrations from the Eurasian to the Canadian Basin, toward the Beaufort Gyre freshwater center. In this region, where river input and Pacific Water compose a significant fraction of surface freshwater, meltwater estimates are likely too high. Note that the same relationship also holds in the Amundsen Basin and likely represents the influence of Canadian Basin waters as discussed previously. The positive correlation suggests the need for additional research on the partitioning of gases in ice melt/freeze processes.

In the Canadian Basin, the greatest under ice peak in biological activity near the Mendeleev Ridge (6 September, around 2500 km, Figure 3) corresponds to the region of highest light transmittance through thin melt-pond rich first year ice [Nicolaus *et al.*, 2012]. Estimates and models of Arctic productivity currently assume no under ice production but blooms fed by sufficient light transmittance through ice have been documented in recent years [Arrigo *et al.*, 2012; Mundy *et al.*, 2009]. There is no evidence in the hydrographic data for dynamically driven nutrient increases over the ridge. A relatively long residence time of surface waters in the Canada Basin and consolidated ice cover limiting gas exchange complicate interpretations of saturation state because they represent the cumulative effect of changes over a long period of time.

## 5. Summary and Implications

Overall we see that biological processes dominate the mean total oxygen saturation in the surface waters under ice cover in the Arctic; however, there is substantial interbasin variability and some important deviation from this mean trend. In the Nansen Basin, physical oxygen is undersaturated (i.e.,  $\Delta Ar < 0$ ) and biological oxygen is supersaturated (i.e.,  $\Delta(O_2/Ar) > 0$ ). The anticorrelation between  $\Delta Ar$  and  $\Delta(O_2/Ar)$  observed in this region is consistent with a shared controlling mechanism. Ice melt, cooling, and vertical mixing would lead to the observed undersaturated Ar, while in situ biological production in the ice-free regions with sufficient AW derived nutrients is consistent with the observed biological supersaturations. Further into the central Arctic, Ar is supersaturated up to 3% and  $\Delta(O_2/Ar)$  averages 4.9%. Ar supersaturation is likely a result of freezing in the central Arctic, and inefficient exchange with the atmosphere in ice-covered regions, while under ice peaks in  $\Delta(O_2/Ar)$  correspond to regions of lower ice concentrations where light transmittance is higher. It is also possible that interbasin  $\Delta Ar$  variability could be reflecting net freeze in the Canadian Basin and net melt in the Nansen Basin, thus tracing net transport of meltwater from the Pacific to the Atlantic side of the upper Arctic Ocean via ice drift.

While vertical mixing of AW does not currently appear to be a major driver of recent observed summer sea ice loss, it is possible that with reduced ice cover and increased wind-energy input there could be increased upward mixing of AW in the NB. Higher seasonal meltwater content would likely create stronger Ar undersaturations in the NB. Future studies should aim at improving estimates of the influence of meltwater on Ar saturation. It is unclear how biology will respond to a change in AW expression at the surface. Considering that the upper Arctic is often oligotrophic [Arrigo *et al.*, 2008], enhanced mixing of AW would not only provide nutrients but increase light availability through melting of sea ice.

The observed and predicted reductions in thick multiyear ice could allow for seasonal equilibration of gases with the atmosphere and thus less extreme oxygen supersaturations. We see signs of likely increased

productivity occurring under the ice where there is sufficient light transmission. The predicted continued shift toward a higher proportion of first year ice will support increased blooms and it will become increasingly important for under ice biological activity to be accounted for in estimates and models of total Arctic Ocean productivity and carbon cycling.

#### Acknowledgments

We thank two anonymous reviewers for their thoughtful comments. Data for this paper are available at <http://www.bco-dmo.org> and [www.pangaea.de](http://www.pangaea.de). This material is based upon work supported by the National Science Foundation, Graduate Research Fellowship Program under grant 1106401. M.-L.T. was supported in part by the National Science Foundation, Division of Polar Programs award ARC-1107623. N.C. was partly funded by an Alfred P. Sloan fellowship.

#### References

- Anderson, D. L. (1961), Growth rate of sea ice, *J. Glaciol.*, *3*, 1170–1172.
- Arrigo, K. R., G. van Dijken, and S. Pabi (2008), Impact of a shrinking Arctic ice cover on marine primary production, *Geophys. Res. Lett.*, *35*, L19603, doi:10.1029/2008GL035028.
- Arrigo, K. R., et al. (2012), Massive phytoplankton blooms under Arctic sea ice, *Science*, *336*(6087), 1408–1408.
- Boetius, A., et al. (2013), Export of algal biomass from the melting Arctic sea ice, *Science*, *339*(6126), 1430–1432.
- Carmack, E., D. Barber, J. Christensen, R. Macdonald, B. Rudels, and E. Sakshaug (2006), Climate variability and physical forcing of the food webs and the carbon budget on panarctic shelves, *Prog. Oceanogr.*, *71*(2–4), 145–181.
- Cassar, N., B. A. Barnett, M. L. Bender, J. Kaiser, R. C. Hamme, and B. Tilbrook (2009), Continuous high-frequency dissolved O<sub>2</sub>/Ar measurements by Equilibrator Inlet Mass Spectrometry, *Anal. Chem.*, *81*(5), 1855–1864.
- Cassar, N., P. J. DiFiore, B. A. Barnett, M. L. Bender, A. R. Bowie, B. Tilbrook, K. Petrou, K. J. Westwood, S. W. Wright, and D. Lefevre (2011), The influence of iron and light on net community production in the subarctic and Polar Frontal Zones, *Biogeosciences*, *8*(2), 227–237.
- Cleveland, W. S. (1979), Robust locally weighted regression and smoothing scatterplots, *J. Am. Stat. Assoc.*, *74*(368), 829–836.
- Codispoti, L., and F. A. Richards (1971), Oxygen supersaturations in Chukchi Sea and East Siberian Sea, *Deep Sea Res. Oceanogr. Abstr.*, *18*(3), 341–351.
- Craig, H., and T. Hayward (1987), Oxygen supersaturation in the ocean—Biological versus physical contributions, *Science*, *235*(4785), 199–202.
- D'Asaro, E., C. Lee, L. Rainville, R. Harcourt, and L. Thomas (2011), Enhanced turbulence and energy dissipation at ocean fronts, *Science*, *332*(6027), 318–322.
- Ekwurzel, B., P. Schlosser, R. A. Mortlock, R. G. Fairbanks, and J. H. Swift (2001), River runoff, sea ice meltwater, and Pacific water distribution and mean residence times in the Arctic Ocean, *J. Geophys. Res.*, *106*(C5), 9075–9092.
- Emerson, S., and J. Hedges (2008), *Chemical Oceanography and the Marine Carbon Cycle*, xi, 453 p., Cambridge Univ. Press, Cambridge, U. K.
- Falkner, K. K., M. Steele, R. A. Woodgate, J. H. Swift, K. Aagaard, and J. Morison (2005), Dissolved oxygen extrema in the Arctic Ocean halocline from the North Pole to the Lincoln Sea, *Deep Sea Res., Part I*, *52*(7), 1138–1154.
- Fanning, K. A., and L. M. Torres (1991), Rn-222 and Ra-226—Indicators of sea-ice effects on air-sea gas-exchange, *Polar Res.*, *10*(1), 51–58.
- Garcia, H. E., and L. I. Gordon (1992), Oxygen solubility in seawater—Better fitting equations, *Limnol. Oceanogr.*, *37*(6), 1307–1312.
- Garcia, H. E., R. A. Locarnini, T. P. Boyer, J. I. Antonov, M. M. Zweng, O. K. Baranova, and D. R. Johnson (2010), World Ocean Atlas 2009, in *NOAA Atlas NESDIS 71*, vol. 4, *Nutrients (Phosphate, Nitrate, Silicate)*, U.S. Gov. Print. Off., Washington, D. C.
- Hamme, R. C., and S. R. Emerson (2004), The solubility of neon, nitrogen and argon in distilled water and seawater, *Deep Sea Res., Part I*, *51*(11), 1517–1528.
- Hood, E. M., B. L. Howes, and W. J. Jenkins (1998), Dissolved gas dynamics in perennially ice-covered Lake Fryxell, Antarctica, *Limnol. Oceanogr.*, *43*(2), 265–272.
- Horner, R., S. F. Ackley, G. S. Dieckmann, B. Gulliksen, T. Hoshiai, L. Legendre, I. A. Melnikov, W. S. Reeburgh, M. Spindler, and C. W. Sullivan (1992), Ecology of sea ice biota. 1. Habitat, terminology, and methodology, *Polar Biol.*, *12*(3–4), 417–427.
- Jones, E. P., L. G. Anderson, and J. H. Swift (1998), Distribution of Atlantic and Pacific waters in the upper Arctic Ocean: Implications for circulation, *Geophys. Res. Lett.*, *25*(6), 765–768.
- Jones, E. P., L. G. Anderson, S. Jutterstrom, L. Mintrop, and J. H. Swift (2008), Pacific freshwater, river water and sea ice meltwater across Arctic Ocean basins: Results from the 2005 Beringia Expedition, *J. Geophys. Res.*, *113*, C08012, doi:10.1029/2007JC004124.
- Korhonen, M., B. Rudels, M. Marnela, A. Wisotzki, and J. Zhao (2013), Time and space variability of freshwater content, heat content and seasonal ice melt in the Arctic Ocean from 1991 to 2011, *Ocean Sci.*, *9*(6), 1015–1055.
- Lien, V. S., F. B. Vikebo, and O. Skagseth (2013), One mechanism contributing to co-variability of the Atlantic inflow branches to the Arctic, *Nat. Commun.*, *4*, 1488.
- Lind, S., and R. B. Ingvoldsen (2012), Variability and impacts of Atlantic Water entering the Barents Sea from the north, *Deep Sea Res., Part I*, *62*, 70–88.
- Loose, B., W. R. McGillis, P. Schlosser, D. Perovich, and T. Takahashi (2009), Effects of freezing, growth, and ice cover on gas transport processes in laboratory seawater experiments, *Geophys. Res. Lett.*, *36*, L05603, doi:10.1029/2008GL036318.
- Loose, B., W. R. McGillis, D. Perovich, C. J. Zappa, and P. Schlosser (2014), A parameter model of gas exchange for the seasonal sea ice zone, *Ocean Sci.*, *10*(1), 17–28.
- Michel, C., L. Legendre, J. C. Theriault, S. Demers, and T. Vandevelde (1993), Springtime coupling between ice algal and phytoplankton assemblages in Southeastern Hudson-Bay, Canadian Arctic, *Polar Biol.*, *13*(7), 441–449.
- Moore, R. M., and W. Spitzer (1990), Heat-transfer from Atlantic waters to sea ice in the Arctic-Ocean—Evidence from dissolved argon, *Geophys. Res. Lett.*, *17*(12), 2149–2152.
- Moreau, S., M. Vancoppenolle, J. Y. Zhou, J. L. Tison, B. Delille, and H. Goosse (2014), Modelling argon dynamics in first-year sea ice, *Ocean Modell.*, *73*, 1–18.
- Mundy, C. J., et al. (2009), Contribution of under-ice primary production to an ice-edge upwelling phytoplankton bloom in the Canadian Beaufort Sea, *Geophys. Res. Lett.*, *36*, L17601, doi:10.1029/2009GL038837.
- Newton, R., P. Schlosser, R. Mortlock, J. Swift, and R. MacDonald (2013), Canadian Basin freshwater sources and changes: Results from the 2005 Arctic Ocean Section, *J. Geophys. Res. Oceans*, *118*, 2133–2154, doi:10.1002/jgrc.20101.
- Nicolaus, M., C. Katlein, J. Maslanik, and S. Hendricks (2012), Changes in Arctic sea ice result in increasing light transmittance and absorption, *Geophys. Res. Lett.*, *39*, L24501, doi:10.1029/2012GL053738.
- Overland, J., U. Bhatt, J. Key, Y. Liu, and M. Wang (2011), Temperature and clouds, in *Arctic Report Card 2011*. [Available at <http://www.arctic.noaa.gov/reportcard/>]
- Perrette, M., A. Yool, G. D. Quartly, and E. E. Popova (2011), Near-ubiquity of ice-edge blooms in the Arctic, *Biogeosciences*, *8*(2), 515–524.

- Poisson, A., and C. T. A. Chen (1987), Why is there little anthropogenic CO<sub>2</sub> in the Antarctic bottom water, *Deep Sea Res., Part A*, 34(7), 1255–1275.
- Popova, E. E., A. Yool, A. C. Coward, F. Dupont, C. Deal, S. Elliott, E. Hunke, M. B. Jin, M. Steele, and J. L. Zhang (2012), What controls primary production in the Arctic Ocean? Results from an intercomparison of five general circulation models with biogeochemistry, *J. Geophys. Res.*, 117, C00D12, doi:10.1029/2011JC007112.
- Proshutinsky, A., R. Krishfield, M. L. Timmermans, J. Toole, E. Carmack, F. McLaughlin, W. J. Williams, S. Zimmermann, M. Itoh, and K. Shimada (2009), Beaufort Gyre freshwater reservoir: State and variability from observations, *J. Geophys. Res.*, 114, C00A10, doi:10.1029/2008JC005104.
- Rudels, B., E. P. Jones, L. G. Anderson, and G. Kattner (1994), On the intermediate depth waters of the Arctic Ocean, in *The Polar Oceans and Their Role in Shaping the Global Environment*, edited by O. M. Johannessen, R. D. Muench, and J. E. Overland, pp. 33–46, AGU, Washington, D. C.
- Rudels, B., L. G. Anderson, and E. P. Jones (1996), Formation and evolution of the surface mixed layer and halocline of the Arctic Ocean, *J. Geophys. Res.*, 101(C4), 8807–8821.
- Rudels, B., E. P. Jones, U. Schauer, and P. Eriksson (2004), Atlantic sources of the Arctic Ocean surface and halocline waters, *Polar Res.*, 23(2), 181–208.
- Rutgers van der Loeff, M. M., N. Cassar, M. Nicolaus, B. Rabe, and I. Stimac (2014), The influence of sea-ice cover on air-sea gas exchange estimated with radon-222 profiles, *J. Geophys. Res. Oceans*, 119, 2735–2751, doi:10.1002/2013JC009321.
- Schauer, U., and A. Beszczynska-Möller (2009), Problems with estimation and interpretation of oceanic heat transport, Äconceptual remarks for the case of Fram Strait in the Arctic Ocean, *Ocean Sci.*, 5(4), 487–494.
- Schauer, U., B. Rabe, and A. Wisotzki (2012), *Physical Oceanography During POLARSTERN Cruise ARK-XXVI/3*, Alfred Wegener Inst., Helmholtz Center for Polar and Marine Research, Bremerhaven, Germany, doi:10.1594/PANGAEA.774181.
- Shadwick, E. H., B. Tilbrook, N. Cassar, T. W. Trull, and S. R. Rintoul (2014), Summertime physical and biological controls on O<sub>2</sub> and CO<sub>2</sub> in the Australian Sector of the Southern Ocean, *J. Marine Syst.*, doi:10.1016/j.jmarsys.2013.12.008.
- Spitzer, W. S., and W. J. Jenkins (1989), Rates of vertical mixing, gas-exchange and new production—Estimates from seasonal gas cycles in the upper ocean near Bermuda, *J. Mar. Res.*, 47(1), 169–196.
- Spreen, G., L. Kaleschke, and G. Heygster (2008), Sea ice remote sensing using AMSR-E 89-GHz channels, *J. Geophys. Res.*, 113(C2), doi:10.1029/2005jc003384.
- Steele, M., and T. Boyd (1998), Retreat of the cold halocline layer in the Arctic Ocean, *J. Geophys. Res.*, 103(C5), 10,419–10,435.
- Tedesco, L., M. Vichi, and D. N. Thomas (2012), Process studies on the ecological coupling between sea ice algae and phytoplankton, *Ecol. Modell.*, 226, 120–138.
- Timmermans, M. L., R. Krishfield, S. Laney, and J. Toole (2010), Ice-tethered profiler measurements of dissolved oxygen under permanent ice cover in the Arctic Ocean, *J. Atmos. Oceanic Technol.*, 27(11), 1936–1949.
- Top, Z., S. Martin, and P. Becker (1985), On the dissolved surface oxygen supersaturation in the Arctic, *Geophys. Res. Lett.*, 12(12), 821–823.
- Top, Z., S. Martin, and P. Becker (1988), A laboratory study of dissolved noble-gas anomaly due to ice formation, *Geophys. Res. Lett.*, 15(8), 796–799.
- Tremblay, J. E., et al. (2011), Climate forcing multiplies biological productivity in the coastal Arctic Ocean, *Geophys. Res. Lett.*, 38, L18604, doi:10.1029/2011GL048825.
- Uchida, H., T. Kawano, I. Kaneko, and M. Fukasawa (2008), In situ calibration of optode-based oxygen sensors, *J. Atmos. Oceanic Technol.*, 25(12), 2271–2281.
- Ulfso, A., N. Cassar, M. Korhonen, S. van Heuven, M. Hoppema, G. Kattner, and L. G. Anderson (2014), Late summer net community production in the central Arctic Ocean using multiple approaches, *Global Biogeochem. Cycles*, 28, doi:10.1002/2014GB004833.
- Vancoppenolle, M. et al. (2013), Role of sea ice in global biogeochemical cycles: Emerging views and challenges, *Quat. Sci. Rev.*, 79, 207–230.
- Woodgate, R. A., K. Aagaard, R. D. Muench, J. Gunn, G. Bjork, B. Rudels, A. T. Roach, and U. Schauer (2001), The Arctic Ocean boundary current along the Eurasian slope and the adjacent Lomonosov Ridge: Water mass properties, transports and transformations from moored instruments, *Deep Sea Res., Part I*, 48(8), 1757–1792.
- Worby, A. P., C. A. Geiger, M. J. Paget, M. L. Van Woert, S. F. Ackley, and T. L. DeLiberty (2008), Thickness distribution of Antarctic sea ice, *J. Geophys. Res.*, 113, C05S92, doi:10.1029/2007JC004254.
- Zhou, J., B. Delille, F. Brabant, and J.-L. Tison (2014), Insights into oxygen transport and net community production in sea ice from oxygen, nitrogen and argon concentrations, *Biogeosciences*, 11, 5007–5020, doi:10.5194/bg-11-5007-2014.